Supplemental Document

optica

Structural color from a coupled nanowire pair beyond the bonding and antibonding model: supplement

QITONG LI,[1] TONG WU,[2] JORIK VAN DE GROEP,[1] PHILIPPE LALANNE,[2] AND MARK L. BRONGERSMA[1,*]

[1] *Geballe Laboratory for Advanced Materials, Stanford University, Stanford, California 94305, USA*
[2] *LP2N, CNRS, University of Bordeaux, 33400 Talence, France*
[*] *Corresponding author: brongersma@stanford.edu*

Supplement DOI: https://doi.org/10.6084/m9.figshare.14099141

Parent Article DOI: https://doi.org/10.1364/OPTICA.418888

Color generation from a nanowire pair beyond bonding and anti-bonding model

QITONG LI[1], TONG WU[2], JORIK VAN DE GROEP[1], PHILIPPE LALANNE[2], AND MARK L. BRONGERSMA[1*]

[1]*Geballe Laboratory for Advanced Materials, Stanford University, Stanford, CA 94305, USA.*
[2]*LP2N, CNRS, University of Bordeaux, 33400 Talence, France.*

**brongersma@stanford.edu*

Methods:

Numerical simulations. We perform 2D simulations using the mode solver of the commercial software package COMSOL. In the quasinormal mode (QNM) simulations, the simulation area is defined as a circle with a radius of 600 nm surrounded by a 300-nm-thick perfect matching layer (PML). The scattering field simulations for single NW and NW pairs are performed in a 1.6 μm box with 200-nm-thick PML surrounding it. The full-field profile used to calculate α_{sim} and thereby retrieve the coupling coefficient κ is then calculated by summing up the scattering field and the background incident field. In the full-field simulations, we apply periodic boundary conditions and two ports along the light propagation direction to simulate the properties of the arrays. To simplify the analysis of the resonant modes, Si NWs are all suspended in the air with a constant refractive index of 4 in QNM and scattering efficiency simulations except Fig. 3c. In Fig. 3c and supplementary Fig. 4, Si NWs are placed on a sapphire substrate. The refractive index of sapphire is set as 1.77, and the real dispersion and optical absorption of Si are included in the simulations.

Sample fabrication. We start the fabrication with a 1 cm square 500-nm-thick single-crystalline Si on sapphire substrate that is commercially available from MTI-Corp. The thickness of the Si slab is thinned down to 50 nm by reactive ion etching (Lam Research TCP 9400 Poly Etcher). A 70 nm thick hydrogen silsesquioxane (HSQ) layer, serving as a negative-tone electron beam resist, is then spin-coated on the Si slab, and a conductive polymer layer (E-Spacer 300Z) is also spin-coated to reduce the electron charging effects in the nonconductive substrate during the electron beam exposure. The electron beam lithography is then performed using a JEOL 6300 100 kV system. The chosen beam current is 1 nA and the base electron beam dose is set to ~2000 μC/cm^2. The development is then performed in 25% tetramethylammonium hydroxide for 2 mins. Finally, reactive ion etching is used again to transfer the HSQ hard mask patterns into the Si slab, and the remaining HSQ hard mask pattern is removed by wet-etching in a 2% hydrogen fluoride solution for 1 min.

Optical measurements. We perform the optical scattering measurement using a Nikon C2 confocal microscope. Light from a halogen lamp is first polarized 45° with respect to the NW orientation and top-illuminated through a ×20 objective (Nikon CFI Achro LWD 20X, NA = 0.4, working distance = 3.9 mm) for bright-field reflection measurements. The reflection signal is then collected by the same ×20 objective (NA = 0.4) and polarization-filtered by the second polarizer orthogonal to the first one for cross-polarized detection. The reflection optical images of the samples are taken by a Nikon DS-Fi1 camera. A confocal scanner with a 30 μm pin hole is used to spatially select the signal which is analyzed using a SpectraPro 2300i spectrometer (150 lines/mm, blazed at λ = 500 nm) and Pixis Si CCD (−70 °C detector temperature). The reported spectra are the average of 10 frames (4 s integration time each). The dark spectrum is subtracted and all reflection spectra are normalized by the reflection spectra of a protected silver mirror (Thorlabs, PF10-03-P01) to correct the system response.

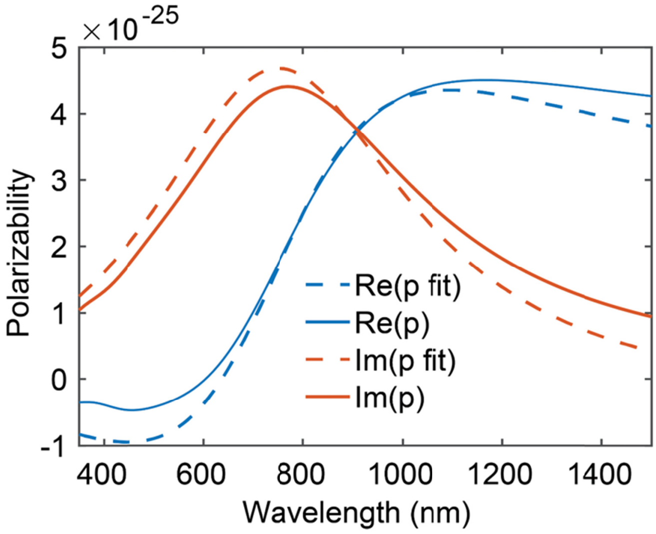

Figure S1. Modeling of a single NW as a linear electric dipole. Integrated (solid lines, obtained from the equation $\alpha_{\text{sim}} = \int \varepsilon_0(\varepsilon - 1)\frac{E(\mathbf{r})}{E_{\text{inc}}(\mathbf{r}=0)}dS$) and fitted (dashed lines, obtained from the equation $\alpha = \frac{-i\kappa}{\tilde{\omega}_0 - \omega}$) effective polarizability of a 50 nm sized square Si (refractive index = 4) NW as a function of the incident wavelength.

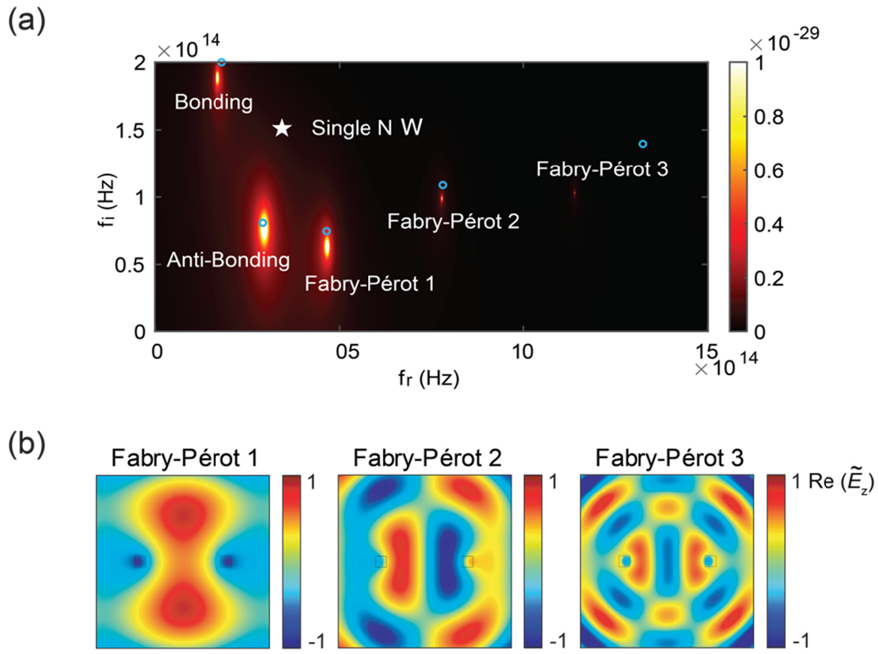

Figure S2. Higher-order Fabry-Pérot modes in a NW pair. (a) Calculated reciprocal of the determinant of the 2×2 matrix used to describe the coupled NW (dipole) system $1/\det(A(\omega))$ as a function of the real and imaginary part of the complex eigen frequency. The distance between the two NWs is 400 nm. The complex frequencies of the QNMs retrieved from numerical simulations are overlaid as blue circles. The complex frequency of TM_{11} mode for single NW (white star) is also shown for reference. (b) Out-of-plane electric field distribution of the three simulated eigen modes of a 50 nm sized square Si (refractive index n = 4) NW pair with a 400 nm wire spacing.

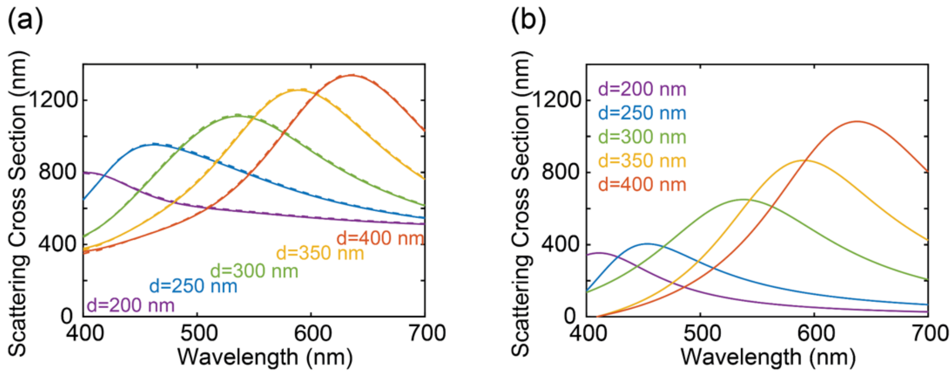

Figure S3. Quasi normal mode (QNM) reconstruction. (a) QNM reconstructed (solid lines) and simulated (dashed lines) scattering cross section of a NW pair as a function of the incident wavelength. (b) The scattering cross section contribution from the Fabry-Pérot mode in a NW pair as a function of the incident wavelength.

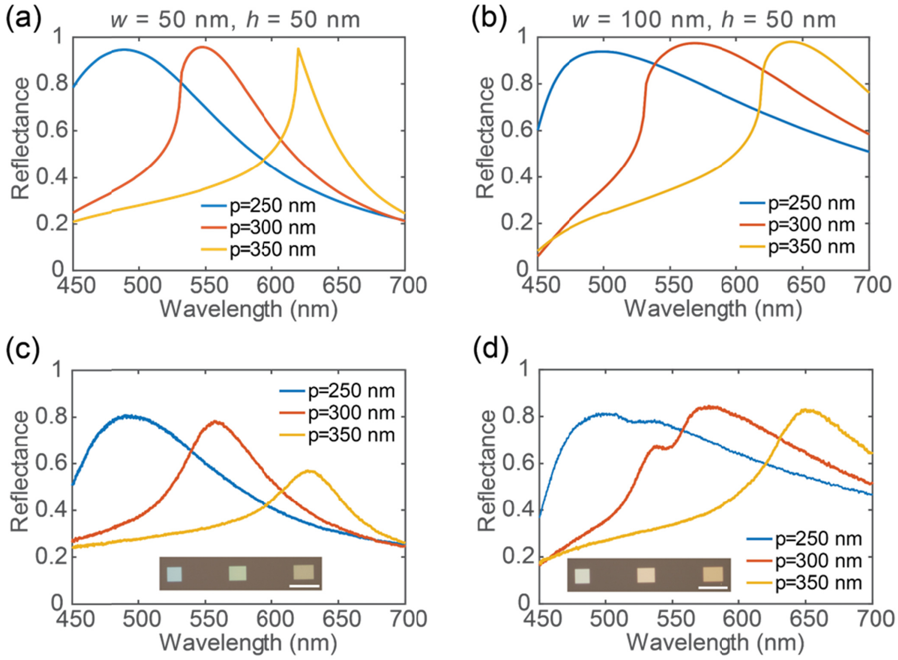

Figure S4. NW array as a meta-mirror under normal incident light (at Γ point). (a, b) Simulated and (c, d) measured reflection spectra under TM polarized illumination for NW arrays with different periods. NW dimensions are chosen as (a, c) w = 50 nm, h = 50 nm and (b, d) w = 100 nm, h = 50 nm. A ×4 objective (NA = 0.1) is used to collect the signal. Insets: reflection optical images of the fabricated NW arrays under a TM-polarized white-light illumination. Scale bar: 100 μm.

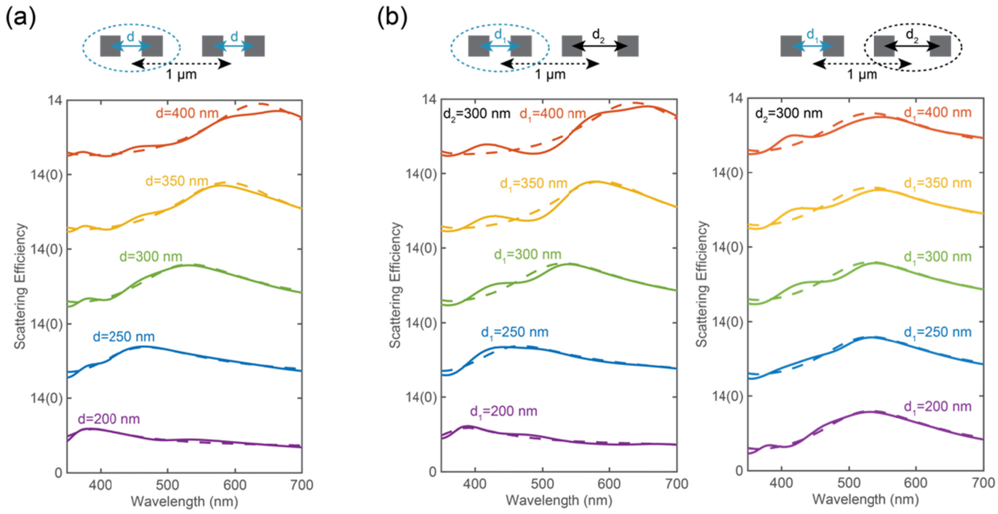

Figure S5. Coupling effects between neighboring NW pairs. (a) Two identical NW pairs side by side with 1 μm inter-spacing. Solid lines: simulated scattering efficiency spectra of one NW pair with different intra-spacings (d = 200 nm - 400 nm). Dashed lines: simulated scattering efficiency spectra of an isolated NW pair with the same geometry. NW pairs are under normally-incident TM polarized illumination. (b) Two non-identical NW pairs side by side with 1 μm inter-spacing. Solid lines: simulated scattering efficiency spectra of each NW pair. The inter-spacing of the left NW pair changes gradually (d = 200 nm - 400 nm), while it keeps as a constant number (d = 300 nm) for the right NW pair. Dashed lines: simulated scattering efficiency spectra of an isolated NW pair with the same geometry.

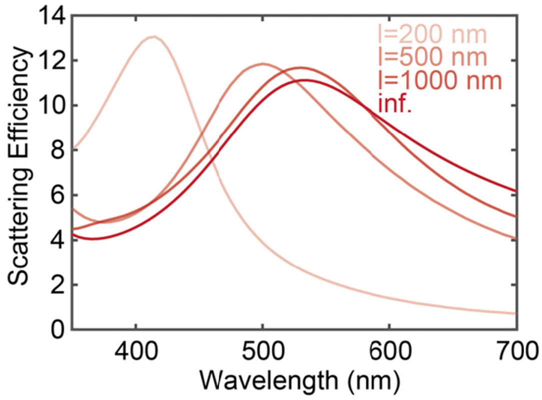

Figure S6. Influence of the length of NWs to the scattering properties of the proposed Si NW pair system. The figure shows the simulated scattering efficiency spectra of Si NW pairs with different NW lengths (from 200 nm to infinitely long). The NW separation distance is set as 300 nm.